

pubs.acs.org/JPCB Article

# Characterizing Rotational Dynamics and Heterogeneity via Single-Molecule Intensity Measurements

Published as part of The Journal of Physical Chemistry B special issue "Mark Ediger Festschrift".

Alec R. Meacham, Jaladhar Mahato, Han Yang, and Laura J. Kaufman\*



Cite This: J. Phys. Chem. B 2024, 128, 9233-9243



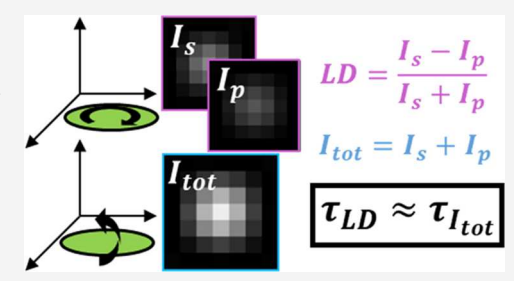
**ACCESS** I

III Metrics & More

Article Recommendations

SI Supporting Information

**ABSTRACT:** Dynamic heterogeneity in glassy systems has typically been characterized at the single-molecule level by extracting rotational relaxation time scales from linear dichroism (LD) collected via two orthogonally polarized channels. However, in such measurements, localization precision is diminished due to photons lost relative to collection in a single detection channel. This poses challenges in characterizing rotational and translational dynamics simultaneously, as translational measurements require high localization precision. In this paper, we present a method for extracting rotational dynamics of glassy systems at the single-molecule level from intensity fluctuations of fluorescent probe molecules in a wide-field configuration without the use of a polarizing optical component. Through



numerical analysis, we show that LD and intensity measurements probing rotational dynamics report similar, approximately second-order rotational correlation decays even at low signal to noise. Thus, within the assumptions of small, isotropic rotations, LD and intensity autocorrelation analysis should provide identical information on the time scale and heterogeneity of rotational dynamics. We then present experimental results that validate this numerical result, with direct comparison of LD and intensity-based approaches across probe molecules in both polymeric and small-molecule glass formers as well as across optical configurations. Our results demonstrate moderate correlation on a per-probe basis between rotational time scales obtained from both approaches, with deviations consistent with those expected in a dynamically heterogeneous system. We envision that this easily accessible strategy will be of use across disciplines for characterizing single-molecule rotational dynamics in limited signal situations and/or when high-precision localization is required.

#### INTRODUCTION

Glassy systems have been the subject of intense research over the past several decades due not only to their potential in a wide array of applications from drug delivery to organic electronics but also to their fundamentally interesting properties. Among the unusual and interesting properties frequently observed in glassy systems is an apparent heterogeneity in dynamics, a phenomenon that has been widely reported across both small molecule glass formers and polymeric glass formers near the glass transition temperature  $(T_{\rm g})$ . These heterogeneous dynamics manifest as stretched exponential decays in the correlation functions characterizing rotational dynamics, suggesting a broad array of underlying time scales.

While initial studies of dynamic heterogeneity relied on ensemble measurements, <sup>2,4</sup> single molecule (SM) methods, which can get underneath the ensemble average, are very valuable for teasing out details of spatial and temporal extents of heterogeneity. <sup>5</sup> Typically, in such measurements temporal trajectories of the reduced linear dichroism (LD) of individual fluorescent probe molecules are analyzed to reveal rotational dynamics in small molecule supercooled liquid hosts or segmental dynamics in glassy polymer hosts. <sup>6-10</sup> Such

measurements have also been used to characterize structure of and molecular confinement in mesoporous silica, and static LD measurements have long been used to characterize (bio)molecular structure or transition dipole orientation. In measurements that track changes in LD over time, such as those performed on single molecule probes in supercooled liquids, the autocorrelation function of an individual probe's LD trajectory is typically fit to a Kohlrausch–Williams–Watts (stretched exponential) equation to determine characteristics of rotational dynamics. Assuming the selection of an ideal probe, which is sufficiently long-lived and does not average over spatial heterogeneities in the system, this approach reports information about rotational motion of the probe that in turn reflects the dynamics and extent of heterogeneity of the host. 9,14

Received: March 30, 2024
Revised: August 16, 2024
Accepted: September 5, 2024
Published: September 17, 2024





A phenomenon of interest that is related to dynamic heterogeneity is the rotational-translational decoupling observed as glassy systems approach  $T_{\rm g}$ . <sup>15–18</sup> Near the glass transition, measured dynamics appear to violate the temperature dependence predicted by the Stokes–Einstein and Debye–Stokes–Einstein relationships, and enhancement of translational motion up to several orders of magnitude has been observed. <sup>17</sup> These observations, first reported in ensemble measurements, were postulated to arise due to differences in ensemble averaging as it manifests in measurements of rotational and translational dynamics. <sup>17</sup> Recently, this decoupling was also observed at the SM level, provoking additional questions on the roles of ensemble and time averaging in the origin of this phenomenon. <sup>19</sup>

The simultaneous measurement of rotational and translational dynamics at the SM level was not demonstrated until nearly 20 years after SM observations on rotational dynamics in supercooled liquids were first reported. This was largely due to technical limitations, as the required measurements can easily be achieved in a wide-field configuration, entailing only identification of individual probe locations during LD measurements. Recently, additional experimental approaches that allow simultaneous measurement of single molecule orientation and position have also been demonstrated.<sup>20,21</sup> For any such approach, given the slow translational motion expected near  $T_g$ , to characterize translational mobility in supercooled liquids will require very high localization precision, necessitating the collection of large numbers of photons at each time step. 22,23 Traditional investigation of rotational dynamics at the SM level, through LD, involves splitting probe fluorescence into two orthogonally polarized channels requiring an optical element at which photon loss will occur. In such a configuration, SM position trajectories can be obtained either using one of the two channels, reducing photons by approximately half, or via a summed signal from the two channels, which may introduce additional sources of localization inaccuracy. Identifying a suitable, native single channel alternative to the LD approach would be beneficial not only for monitoring rotational-translational decoupling in glassy systems but for any other application where monitoring rotational and translational dynamics is desirable and measurements are photon-limited, as in SM biological measurements.

To assess alternatives to LD for accessing rotational time scales, we first scrutinize the experimentally detected quantity as it relates to transition dipole orientation. We define the inplane and out-of-plane orientation of the transition dipole by the azimuthal  $(\varphi)$  and polar  $(\theta)$  angles respectively with the z-axis defined along the optical axis. Following Fourkas, the corresponding intensities in the two orthogonal channels,  $I_{\rm s}$  and  $I_{\rm p}$ , are given by eqs 1 and 2.<sup>24</sup>

$$I_{\rm s} \propto (A + B \sin^2 \theta + C \sin^2 \theta \cos 2\varphi)$$
 (1)

$$I_{\rm p} \propto (A + B \sin^2 \theta - C \sin^2 \theta \cos 2\varphi)$$
 (2)

Here A, B, and C are constants that depend on  $\alpha$ , a function of numerical aperture (NA) of the objective lens employed and the refractive index of the medium (n) via  $\alpha = \sin^{-1}(\mathrm{NA}/n)$ . Linear dichroism is defined in eq 3, as explored in Wei et al. and Mackowiak et al. 10

$$LD = \frac{I_{s} - I_{p}}{I_{s} + I_{p}} = \frac{C \sin^{2} \theta}{A + B \sin^{2} \theta} \cos 2\phi$$
(3)

While LD is clearly tied to dipole orientation, it is not straightforwardly associated with a rotational correlation function of a particular rank. Rotational correlation functions, C(t), can be represented as a weighted sum of correlation functions of rank-l,  $C_l(t)$ , via

$$C(t) = \sum_{l} a_{l} C_{l}(t) \tag{4}$$

where  $a_b$  defined and discussed further in eq 10, represents the coefficient associated with the relevant Legendre polynomial.25 For isotropic rotational diffusion, each  $C_l(t)$  exhibits monoexponential decay, with  $C_l(t) = e^{-l(l+1)D_rt}$ , where  $D_r$  is the rotational diffusion coefficient. While ensemble anisotropy measurements report correlations that are purely second order (l=2) and decay as a single exponential for isotropic rotational diffusion, correlation functions of LD include contributions from higher order Legendre polynomials that depend on NA.<sup>25-27</sup> These higher order contributions to the LD correlation function can lead to nonexponential decays even in the presence of homogeneous isotropic rotational dynamics. Specifically, in the low NA limit, A approaches zero and  $B \approx C$ ; thus, LD  $\approx \cos 2\varphi$  and C(t) deviates significantly from single exponential behavior. 25,27 However, with high NA objectives suitable for SM experiments, correlation functions of LD are dominated by second order harmonics (l = 2) as the polar angle contributions are reintroduced and can be characterized by the rotational correlation time constant  $\tau_c = 1/6D_r^{25,27}$  As such, autocorrelations of LD as captured in wide-field SM experiments are expected to report approximately monoexponential decay for homogeneous isotropic rotations, and deviation from this behavior, in the form of a stretched exponential decays, is an indicator of heterogeneous dynamics. 1,25,27

Since LD cannot fully determine the three-dimensional orientation of a probe molecule, a variety of studies have explored how to retrieve this information including via PSF engineering, defocused imaging, or incorporation of a third polarization detection channel.<sup>28–33</sup> However, to investigate the characteristics of rotational dynamics, a compelling alternative to LD is adopting a simpler rather than more complex measurement scheme. In particular, rotational dynamics can be obtained from observed intensity fluctuations of fluorescent probes acquired in a single-channel configuration,<sup>7</sup> offering the additional advantage of circumventing the diminished localization accuracy associated with detection in two (or more) polarization channels. The total emission intensity in a single detection channel can be obtained by summing eqs 1 and 2, with this quantity varying solely with the polar angle (eq 5).

$$I_{\rm em} \propto (A + B \sin^2 \theta) \tag{5}$$

While LD does not explicitly depend on excitation efficiency due to normalization, the total detected intensity depends explicitly on an excitation term with the same form as the emission term but with potentially distinct coefficients depending on how excitation is performed. The total detected intensity is given by eq 6 where  $A_x$  and  $B_x$  are determined by the excitation optics and configuration. <sup>10,34</sup>

$$I_{\text{det}} \propto (A_x + B_x \sin^2 \theta)(A + B \sin^2 \theta)$$
 (6)

Here, we show that correlations of intensity fluctuations, like LD, are dominated by  $C_2(t)$  for experimentally relevant wide-

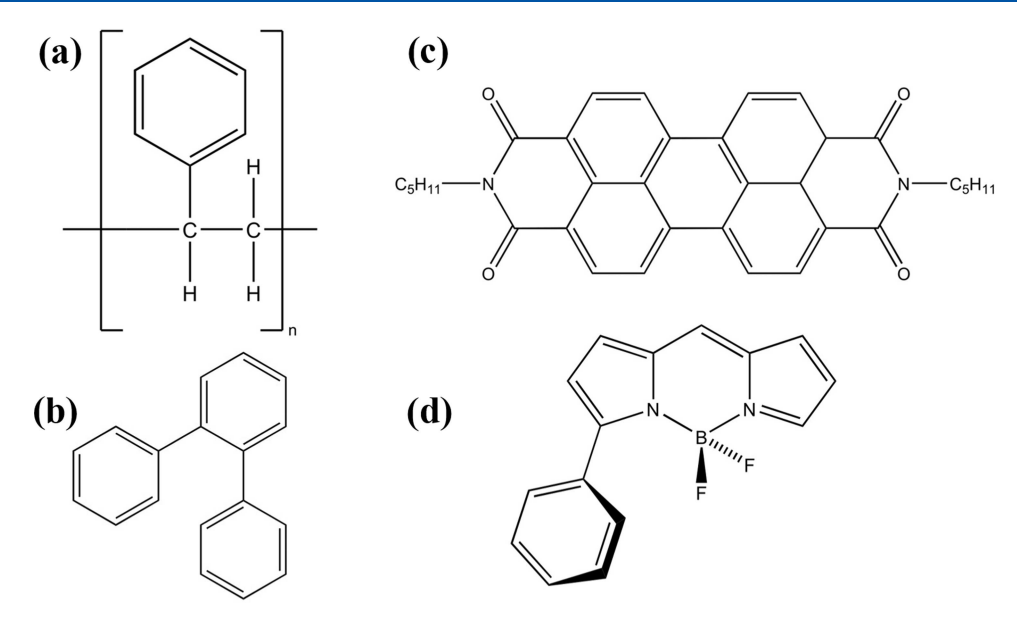


Figure 1. Chemical structures of hosts ((a) PS, (b) OTP) and fluorescent probes ((c) pPDI, (d) BODIPY268) employed.

field optical configurations and demonstrate that single channel intensity fluctuations are expected to report the same rotational dynamics time scales and degree of heterogeneity as captured via traditional LD measurements. Whether this approach then returns the same information as LD in experiment will depend largely on whether probe rotation is isotropic and whether the optical setup is sufficiently and similarly sensitive to probes that are oriented along the optical axis, where total measured intensity decreases. The robustness of the intensity fluctuation approach is demonstrated in high molecular weight polystyrene as well as in the small molecule glass former oterphenyl (OTP) using two different fluorescent probes and across optical configurations. The excellent agreement observed suggests that (1) the method is robust across hosts and probes with varying molecular anisotropy and (2) for typically employed objectives, out-of-plane sensitivity is sufficient for intensity fluctuations to reliably report rotational dynamics. Thus, utilizing intensity fluctuations to extract rotational dynamics serves as a simple alternative to the typically employed LD approach and is particularly useful when minimizing localization uncertainty is desired.

## METHODS

**Sample Preparation.** In this study, we present results from new analysis on three sets of data, two of which were previously published. In particular, we present data from ref 9 on BODIPY268 in o-terphenyl (OTP), data from ref 19 on N,N'-dipentyl-3,4,9,10-perylenedicarboximide (pPDI) in polystyrene, and new data on pPDI in polystyrene, differing from the previously published data in that it was acquired using a lower NA = 0.75 objective lens. Probe and host systems are shown in Figure 1. Details on sample preparation for published data can be found in refs 9 and 19; for the unpublished data, sample preparation largely follows that described in ref 19.

Briefly, atactic polystyrene (PS,  $M_{\rm w}=168$  kg/mol, PDI = 1.05) was purchased from Polymer Source and reprecipitated in toluene before being dissolved in toluene at  $\approx$ 3.5 wt % concentration. The solution was then photobleached in a highpower LED setup to ensure minimal fluorescent impurities in the host polymer.<sup>35</sup> The fluorescent dye, pPDI, was purchased

from Sigma-Aldrich, dissolved in toluene and subsequently added to aliquots of the PS solution to yield a solution with a probe concentration on the order of 10<sup>-11</sup> M. This probe concentration allows for several hundred features to be analyzed per field of view while also minimizing the occurrence of probes colocalized within the same diffraction limited spot. The solution was spin-coated at 3000 rpm onto 7 mm  $\times$  7 mm silicon wafers that had been cleaned with piranha solution (2:1 H<sub>2</sub>SO<sub>4</sub>:H<sub>2</sub>O<sub>2</sub>). The resulting films were at least 200 nm thick as measured by ellipsometry such that observed dynamics are expected to be dominated by bulk behavior.<sup>36</sup> Spin-coated films were annealed in a cryostat chamber (Janis ST-500) at approximately 381 K under vacuum at ~4.5 mTorr for 30 min to remove residual toluene solvent. The cryostat temperature was then lowered to the desired measurement temperature and the system allowed to equilibrate for several hours prior to data collection.

**Imaging.** All data collection was performed using a similar approach, and the full details for the two previously published data sets can be found in refs 9 and 19. For the unpublished data, randomly polarized excitation light was produced by coupling a continuous wave diode Nd:Vanadate laser ( $\lambda = 532$ nm) into a multimode fiber (Newport, F-MCB-T-1FC) shaken by a speaker at constant frequency and amplitude. This light was focused on the back of an objective lens (Zeiss, LD Plan-Neofluar,  $63 \times$ , NA = 0.75) and into the cryostat to illuminate the sample. Fluorescence emission was collected by the same objective in the epi-direction, through a dichroic mirror, a long-pass filter and a bandpass filter. For two-channel experiments, a Wollaston prism was present in the detection path to split the emissions into orthogonally polarized channels that were then imaged on an electron multiplying chargecoupled device camera (EMCCD, Andor iXon DV887). Single-channel movies were collected identically following removal of the Wollaston prism.

Movies were collected at 373.0, 375.8, 377.6, and 380.6 K for PS ( $T_{\rm g} \approx 374.3$  K as measured by differential scanning calorimetry) with frame rates of 0.1, 0.5, 5, and 10 Hz, respectively. These frame rates were chosen to correspond to approximately 10–30 frames per median rotational relaxation

time  $(\tau_{fit})$ , allowing for adequate sampling of the range of dynamic time scales observed at each temperature. An exposure time of 2 s was used for movies with frame rates ≤5 Hz, and movies at higher frame rates were collected with exposure time equal to their respective frame rates. The number of frames collected corresponds to trajectory lengths of  $\gtrsim 200 \tau_{\rm fit}$ , which is sufficiently long to avoid statistical effects on the extracted rotational correlation times that can arise from short trajectories. <sup>29,37</sup> Two-channel data collected on the NA = 0.75 setup described above using a different probe/host system, BODIPY268 in o-terphenyl (previously published in ref 9), was analyzed to demonstrate the robustness of the approach across host systems and fluorescent probes. Additionally, two-channel data (previously published in ref 19) collected on an analogous setup using an objective lens of higher NA (Olympus, M Plan Apochromat MPLAPON, 100x, NA = 0.95) was analyzed to investigate potential differences in perceived rotational time scales due to varying sensitivity to transition dipole orientations near the optical axis as a function of NA.

Data Analysis. Movies acquired in a two-channel configuration were summed to generate effective singlechannel movies using ImageJ in preparation for tracking.<sup>38</sup> In our previous work characterizing SM rotational dynamics, feature positions were identified using an image obtained by summing several hundred frames from the middle of the movie, and probes were assumed to be sufficiently immobile over the course of the full movie such that the same positions were analyzed at all frames.<sup>39</sup> However, probes may undergo appreciable translation over the time scale of experimental acquisition and each single molecule image will not be centered in an identical position throughout the observation time. This translational motion, in conjunction with the existence of dark frames when the probe is either photoblinking or oriented substantially toward the optical axis, means this existing feature finding approach yields many frames without appreciable signal. This is particularly detrimental when performing intensity autocorrelations as, assuming background is relatively consistent, intensity autocorrelation of these frames will manifest in analysis as minimal rotation and affect the perceived dynamics.

To avoid this issue, as well as to facilitate simultaneous characterization of probe rotational and translational dynamics, molecules were localized with an iterative, intensity-weighted centroid method to generate xy-coordinate trajectories using the ImageJ Particle Tracker plugin. 40 While this tracking approach works well for features that are consistently bright, tracking features that are periodically not visible due to photoblinking or orientation toward the optical axis presents challenges. In our data sets, selecting parameters in Particle Tracker that permit linking such trajectories also introduces substantial incorrect linkages, as trajectories from nearby fluorophores are combined. To alleviate this incorrect linking, we instead use a hierarchical clustering method<sup>41</sup> with a user specified displacement cutoff to stitch together short trajectories output from Particle Tracker when generated with a single frame link range. The linked trajectories were then filtered by total number of tracked positions to eliminate trajectories with an insufficient number (<250) of data points, promoting extraction of statistically meaningful rotational time scales.

Extraction of rotational correlation time scales from either LD  $(\tau_{c,LD})$  or intensity  $(\tau_{c,I})$  trajectories was performed using a

custom analysis program written in Python following the general analysis framework described in previous studies.  $^{10,39}$  The signal intensity of each feature at time t was defined by integrating intensities over a  $3 \times 3$ -pixel array about the nearest integer pixel corresponding to the tracked position. For two-channel movies these pixel values were transposed by the width of a single channel to pair features in the s- and p- channels, and the intensities of these paired features,  $I_s$  and  $I_p$ , were used to calculate the LD (eq 3). The time trajectories of either LD or intensity for each feature were utilized to compute the autocorrelation function, C(t) (eq 7), at each time lag using a method available from the Statsmodels library  $^{42}$  with  $a(t) = \text{LD}(t) - \langle \text{LD}(t) \rangle$  or  $a(t) = I(t) - \langle I(t) \rangle$  for two-channel and single-channel movies, respectively.

$$C(t) = \frac{\langle a(t) \cdot a(t+t') \rangle}{\langle a(t)^2 \rangle} \tag{7}$$

The experimental C(t) values were then fit to the Kohlrausch-Williams-Watts stretched exponential function

$$C(t) = C(0)e^{-(t/\tau_{fit})^{\beta}}$$
(8)

using a nonlinear least-squares fitting method from Scipy<sup>41</sup> where C(0) is a prefactor,  $\tau_{\rm fit}$  is the rotational relaxation time, and  $\beta$  is the stretching exponent where  $\beta < 1$  indicates the presence of multiple underlying time scales. These fit parameters were bounded as follows: 0.3 < C(0) < 2.0; frame rate (s)  $< \tau_{\rm fit} <$  movie length (s)/2;  $0.01 < \beta < 2.0$ . Additionally, data was only retained if there were at least 5 points before C(t) decayed below 0.1 and if  $R^2$  of the fit was greater than 0.9. The average rotational correlation time,  $\tau_{c}$  was computed on a per-feature-basis via  $\tau_{c} = (\tau_{\rm fit}/\beta) \cdot \Gamma(1/\beta)$ .

Numerical Computations of Correlation Functions. Rotational correlation functions, C(t), can be represented as a weighted sum of correlation functions of rank-l,  $C_l(t)$  as shown in eq 4. The rank-l correlation functions,  $C_l(t)$ , are defined in terms of the polar angle,  $\theta$ , via

$$C_{l}(t) = \langle P_{l}(\cos[\theta(t)]) \cdot P_{l}(\cos[\theta(0)]) \rangle$$
(9)

where  $P_l$  are the Legendre polynomials. In eq 4,  $a_l$  is calculated based on the angular dependence of the detected experimental parameter via

$$a_{l} = \frac{1}{4\pi} \sum_{m} \left| \int_{0}^{2\pi} \int_{0}^{\pi} \sin\theta \ X(\theta, \varphi) Y_{l,m}(\theta, \varphi) d\theta d\varphi \right|^{2}$$
(10)

where, in our case,  $X(\theta,\varphi)$  is either LD or detected intensity (eqs 3 and 6, respectively) and  $Y_{l,m}$  are the spherical harmonic functions. <sup>26,27</sup>

**Simulations.** Random walks of simultaneous rotational and translational motion for homogeneous, static heterogeneous and dynamic heterogeneous dynamics were simulated. For rotations, the framework presented in Stokely et al. was followed. Briefly, at each simulation step a unit vector was rotated by a solid angle excursion on a sphere sampled from a Rayleigh distribution of width  $\sqrt{2D_r}$ . This simulated isotropic rotation through small step angular displacements should, in the case of homogeneous dynamics, report a monoexponential rotation decay of order l=2. Translational diffusion was sampled similarly, with Cartesian excursions at each time step sampled from a Rayleigh distribution of width  $\sqrt{2D_t}$ . Spherical

Table 1.  $a_l$  Prefactors for NA = 0.95 and 0.75 for LD and Intensity Measurements

	[0, π]		$[\pi/4, 3\pi/4]$			$[0, \pi]$		$[\pi/4, 3\pi/4]$	
	LD, 0.75	Int., 0.75	LD, 0.75	Int., 0.75		LD, 0.95	Int., 0.95	LD, 0.95	Int., 0.95
$a_2$	0.977	0.978	0.950	0.938	$a_2$	0.997	0.995	0.955	0.939
$a_4$	0.022	0.022	0.005	0.036	$a_4$	0.003	0.005	0.014	0.017
$a_6$	$9.70 \times 10^{-4}$	0	0.029	0.014	$a_6$	$1.32 \times 10^{-5}$	0	0.020	0.026
$\Sigma(a_8-a_{20})$	$5.41 \times 10^{-5}$	0	0.015	0.012	$\Sigma(a_8-a_{20})$	$7.54 \times 10^{-8}$	0	0.011	0.019

vector positions and Cartesian coordinates were then used to construct movies for analysis.

Simulated features were initially positioned in a grid such that each simulated feature was 15 pixels away from its nearest neighbors to minimize the likelihood of features crossing during the simulation. A per-channel window size of  $300 \times 300$ pixels was selected resulting in 361 simulated features for each simulation. Initial dipole orientations were randomly generated. For each frame, a 2D Gaussian Point-Spread-Function (PSF) was approximated per-feature about a  $7 \times 7$ -pixel area centered on the nearest integer pixel of the simulated position at time t,  $(x_t, y_t)$ . The intensity contribution for each pixel in this area was computed using a trapezoidal Riemann sum approximation of the integral of the 2D Gaussian centered on  $(x_t, y_t)$  with integration bounds dictated by the respective pixel edges. Contributions of intensity in each orthogonally polarized channel, akin to experimental LD acquisition, were computed following eqs 1 and 2 (NA = 0.95, n = 1.0), with the inclusion of an excitation term as shown in eq 6 (NA = 0.001, n = 1.0). Simulated movies were then tracked and analyzed as described above. Example simulated movies are provided in the Supporting Information (Videos S4, S5).

## ■ RESULTS AND DISCUSSION

We first evaluated the correlation function prefactors,  $a_l$ , for l up to 20 of the correlation functions associated with LD and detected intensity for air objectives (n=1.0) with NA = 0.75 and NA = 0.95 to match those used in the experimental studies (Table 1). Additionally, prefactors were computed for an oil immersion objective of NA = 1.42 (n=1.5) to consider cases where such objectives are appropriate (Table S1). Since the  $a_0$  term corresponds to l=0, this term does not contribute to the C(t) decay but instead is a constant. As such, the  $a_l$  values presented are normalized ignoring  $a_0$ . Odd  $a_l$  values are also omitted from the table as they are zero due to symmetry. Both intensity and LD report a predominantly l=2 correlation function for both NA values when examined over the full polar angular range  $[0, \pi]$ , mirroring results reported previously for analogous calculations on LD.  $^{10,25,29}$ 

While these initial computations assume the ability to image probe molecules across the full range of polar angles, dipole orientations near the optical axis may not be detectable, owing in part to the  $\sin^2\theta$  dependence of excitation efficiency (eq 6), with dipoles oriented near the optical axis experiencing only minimal excitation in a wide-field excitation configuration. The effect of this excitation term is made apparent in Figure 2, in which a steep drop-off in detected intensity as the dipole approaches the optical axis is seen. Additionally, collection efficiency is significantly reduced for these orientations near the optical axis. This can be mitigated through the use of high NA objective lenses, with an NA = 0.95 objective lens collecting approximately 3.5× as many photons for a dipole oriented near the optical axis when compared with an NA = 0.75 objective lens (Figure 2 inset). It is thus expected that in

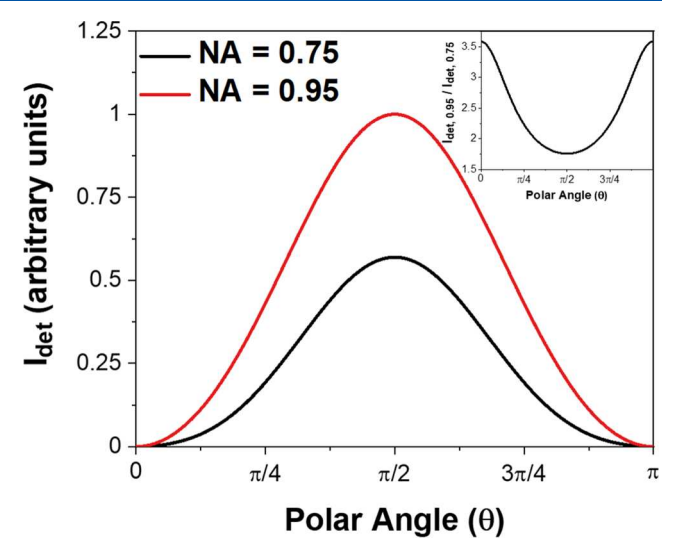


**Figure 2.** Detected intensity,  $I_{\text{dev}}$  as a function of transition dipole polar angle assuming an index of refraction n=1 for wide-field excitation and epi-detection through objective lenses with (black) NA = 0.75 and (red) NA = 0.95. Values are normalized relative to the NA = 0.95 maximum computed intensity. (Inset) Ratio of detected intensity for NA = 0.95 relative to NA = 0.75 as a function of polar angle. The higher NA objective collects ≈3.5× as many photons relative to the lower NA objective at angles near the optical axis.

experimentally relevant conditions the range of accessible polar angles will be limited, but with higher NA objectives accessing a greater range of dipole orientations.

To account for this limitation,  $a_l$  values were also computed for a truncated polar angle range. An experimentally relevant range was approximated by first taking normalized intensity curves, akin to those presented in Figure 2, and scaling each such that the respective peak matches the observed maximal experimental feature intensity with average background subtracted. The average background intensity was then added to all points along the curve and minimum tracked intensity trajectory values from experiment were used to estimate the accessible polar angle range. For NA = 0.75, the limiting case, this range was determined to be slightly broader than  $[\pi/8, 7\pi/8]$  while for NA = 0.95 this range was slightly broader than  $[\pi/16, 15\pi/16]$ . In an effort to account for more limiting cases, which may emerge if signal-to-noise and/or signal-to-background are inferior, a range of  $[\pi/4, 3\pi/4]$  is considered.

In the limited range of  $[\pi/4, 3\pi/4]$ , correlation functions of both intensity and LD show a decrease in the percentage contribution of  $a_2$ , with intensity showing a steeper fall off in  $a_2$  contribution than LD as higher order terms are introduced in the intensity measurement. Despite this, both quantities still show predominant l=2 character and the prefactors for all contributions are quite similar between LD and intensity, particularly for NA = 0.95. Taken together, the calculations

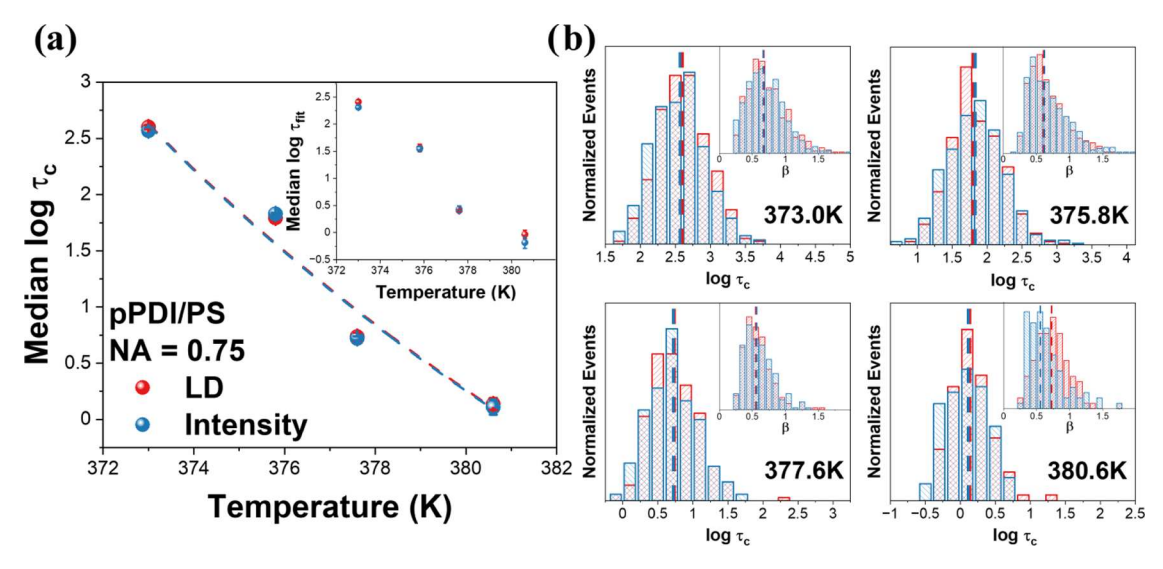


Figure 3. Median (a)  $\tau_c$  and (inset)  $\tau_{fit}$  values derived from (red) LD measurements and (blue) intensity measurements of pPDI in PS for an NA = 0.75 objective lens. Error bars are standard deviations over the three movies analyzed. The colored dashed lines are the fits of the LD and intensity  $\tau_c$  respectively to the VFT equation. These fits report *y*-offsets of 0.813 and 0.803 decades for  $\tau_{c,LD}$  and  $\tau_{c,b}$  respectively both with  $R^2 > 0.95$ . (b) Normalized distributions of  $\tau_c$  and (insets)  $\beta$  derived from (red) LD and (blue) intensity fluctuations for NA = 0.75. Dashed lines indicate median values.

show that intensity and LD fluctuations are expected to report primarily monoexponential C(t) decay with l=2 for isotropic, homogeneous rotational diffusion. As a result, even accounting for potential limitations in the polar angles accessible in widefield fluorescence imaging, rotational characteristics extracted from intensity fluctuations should match those extracted from LD assuming small angle, isotropic probe rotations.

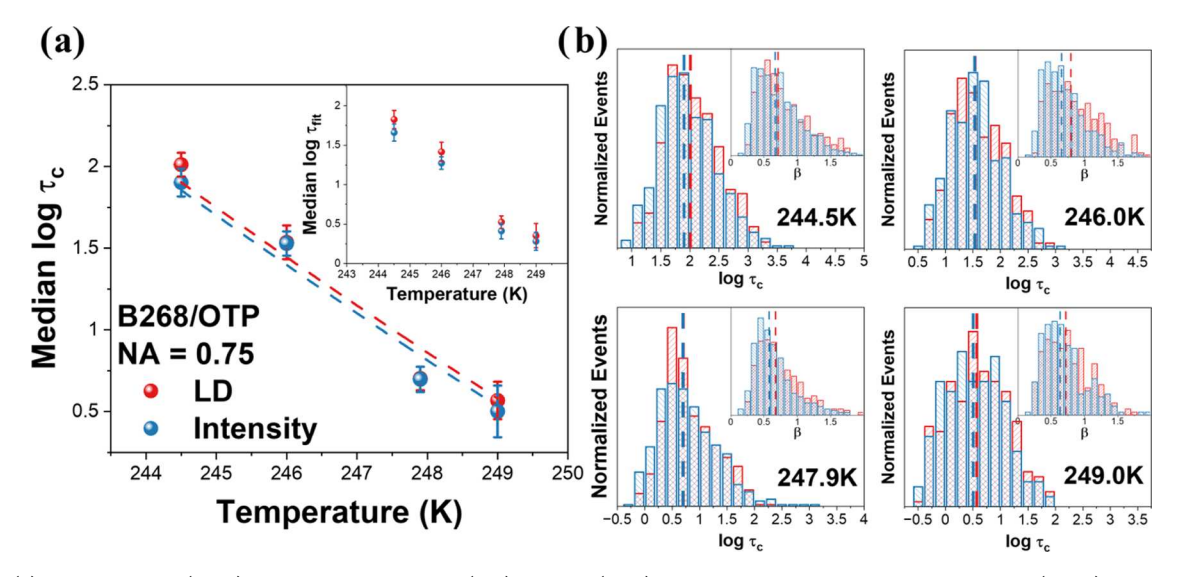
Because the numerical calculations assume small, random isotropic probe rotations, differences between LD and intensity correlation functions may be seen experimentally. To assess the relevance and validity of these numerical results when experimentally examining rotational dynamics of probes, we analyzed several data sets. First, we analyzed SM fluorescence data of pPDI in glassy PS collected using an objective lens with NA = 0.75. This pPDI probe molecule previously has been shown to faithfully report dynamic heterogeneity through LD measurements in PS. Additionally, pPDI is a highly photostable dye that rarely undergoes blinking caused by photophysical processes that could contribute to intensity fluctuations independent of transition dipole rotation. At 44–46 As such, intensity fluctuations from pPDI are expected to result only from molecular reorientation.

First, we confirm that both LD and intensity measurements return the expected temperature dependence of rotational dynamics of the host system. To isolate effects of analysis from those of sample to sample or molecule to molecule variation, unless otherwise specified, all data presented is collected in a two-channel configuration and LD fluctuations are analyzed; the same data is combined into a single channel and intensity fluctuations are analyzed. Even if absolute  $\tau_{\rm c,LD}$  and  $\tau_{\rm c,I}$  are not identical, so long as the probe accurately reports the bulk dynamics of the host, the reported time scales will follow the known temperature dependence of the host rotational dynamics, as typically captured by the Vogel–Fulcher–Tammann (VFT) (eq 10).

$$\log \tau_{\rm c} = \frac{B}{T - T_0} + \log \tau_0 + y \tag{11}$$

This empirical formula captures the temperature dependence of ensemble dielectric measurements of high molecular weight polystyrene and previous, single molecule LD measurements of pPDI in the same host with B = 414.15 K,  $T_0 = 341.3$  K, and  $\log \tau_0 = -11.25$ . An offset (y) is included to account for the fact that probe  $\tau_c$  may not match host (segmental) relaxation time, due to size differences between the pPDI probe and relevant segmental size of the polymeric host. We find that median  $\tau_{c,LD}$  and  $\tau_{c,I}$  show excellent agreement not only with expected host temperature dependence but also in absolute time scale (Figure 3a) though a small, nonsystematic difference is observed, with median  $au_{\mathrm{c,I}}$  values within 10% of median  $au_{\mathrm{c,LD}}$ values. Data acquired natively in a single channel optical configuration shows comparable agreement (Figure S1a) confirming that rotational dynamics can be accurately captured by per-feature intensity fluctuations and reports the expected results from numerical analysis of isotropic probe rotation.

In addition to evaluating median rotational correlation times that allow comparison to previous (probe-bearing or probefree) ensemble studies, SM experiments permit examination of the breadth of time scales present in the system as revealed by distributions of  $\tau_c$ . These  $\tau_c$  distributions reflect the differences in the observed rotational dynamics experienced between molecules over the same interrogated time, i.e., the spatial variation of dynamics present. Figure 3b shows very similar distributions for  $au_{ ext{c,LD}}$  and  $au_{ ext{c,I}}$  at all temperatures, suggesting a comparable breadth of dynamics sampled with both approaches. While the breadth of observed rotational relaxation times, as reflected in the  $\tau_c$  distribution, is one way of assessing heterogeneity in the system, the degree of temporally heterogeneous behavior can also be assessed by examining single molecule  $\beta$  values, as defined by the Kohlrausch-Williams-Watts stretched exponential (eq 8). This quantity serves as a measure of the range of time scales a single molecule experiences during the length of its tracked trajectory, with homogeneous dynamics indicated by a  $\beta$  value of 1.0 and decreasing  $\beta$  values indicative of an increase in the range of underlying time scales contributing to the decay. It is important to note that  $\beta$  values are quite sensitive to trajectory



pubs.acs.org/JPCB

Figure 4. (a) Median  $\tau_c$  and (inset)  $\tau_{\rm fit}$  values derived from (red) LD and (blue) intensity measurements for BODIPY268 (B268) in OTP with NA = 0.75. Error bars are standard deviations from the movies analyzed. The colored dashed lines are the fits of the corresponding data to the VFT equation for OTP rotational time scales derived from dielectric spectroscopy where B = 1820 K,  $T_0 = 168$  K and log  $\tau_0 = -22.5$ . VFT fits with these parameters yielded offsets of 0.612 and 0.564 decades for  $\tau_{c,\rm LD}$  and  $\tau_{c,\rm I}$  derived fits, respectively. (b) Normalized distributions of  $\tau_c$  and (insets) β derived from (red) LD and (blue) intensity fluctuations. Dashed lines indicate median values.

length and artificially broad distributions of  $\beta$  have been reported even in the presence of homogeneous dynamics.  $^{37,51}$  The median  $\beta_{\rm LD}$  and  $\beta_{\rm I}$  values (Figure 3b insets, vertical dashed lines) show good agreement with each other and previous measurements in polystyrene. Moreover,  $\beta$  distributions (Figure 3b insets) look very similar across the two techniques, with the minor deviation in the 380.6 K data attributed to the low signal-to-noise of these movies that makes feature tracking difficult. The consistent agreement between median values and distributions of  $\tau_{\rm c}$  and  $\beta$  obtained from LD and intensity fluctuations indicates that intensity measurements report the same information on rotational dynamics as LD measurements for pPDI in PS.

The validity of the intensity approach for extracting rotational correlation times was further examined through its application to a different probe/host system, with the probe BODIPY268 in the small molecule supercooled liquid oterphenyl (OTP,  $T_{\rm g} \approx 243$  K, data previously published in ref 9). This was done, in part, to ascertain whether the small differences observed between  $\tau_{c,LD}$  and  $\tau_{c,I}$  for pPDI in PS may arise from anisotropy related to the probe and/or host. BODIPY268 is substantially more isotropic than pPDI and, if probe anisotropy contributes to differing time scales between LD and intensity measurements, BODIPY268 would be expected to report a lesser deviation between the two approaches. Moreover, PS is composed of long molecules that could be oriented in a particular manner due to preparation conditions or the presence of the underlying substrate, potentially imparting preferred directionality to the host and probe molecule and possibly inducing anisotropic rotations. In contrast a small, symmetric host molecule such as OTP is unlikely to induce anisotropic motion in a probe.

We find that, like pPDI in PS, BODIPY268 in OTP shows excellent agreement between LD and intensity measurements with regards to the expected temperature dependence (Figure 4a) and, again, shows good agreement between median  $\tau_{\rm c,LD}$  and  $\tau_{\rm c,I}$ . This supports the assertion that probe anisotropy and/or host polymer network influences are not an important factor

leading to the minor differences in median  $au_{c,LD}$  and  $au_{c,I}$  for pPDI in PS data. Instead, these small differences are likely the result of statistical error, a limitation inherent in SM measurements. This issue is exacerbated for BODIPY268 in OTP, as highlighted by the larger error bars in Figure 4a compared to Figure 3a, as BODIPY268 has relatively poor fluorescence efficiency compared to pPDI. (Representative videos of pPDI in PS for both NAs and BODIPY in OTP are shown in Videos S1-S3). This results in inferior signal-tonoise images for the same exposure times and excitation powers, limiting tracking capability and decreasing sensitivity to transition dipoles oriented near the optical axis. As such, these trajectories are more likely to be sparse, which can impact quality and fit of the correlation function. Even so, medians and distributions of  $\tau_{\rm c}$  and  $\beta$  are comparable between the LD and intensity approaches with both successfully probing rotational correlation times and heterogeneity experienced by the probes in this system.

Both data sets presented above were collected with a relatively low NA objective; as discussed above and captured in eqs 5 and 6 as well as Figure 2, the relative sensitivity of a microscope to dipoles with orientations approaching the optical axis is dependent on the NA of the objective lens (Figure 2, inset). As such, molecules are expected to be more readily identified and tracked over a broader range of polar orientations when using higher NA objectives. Thus, it is important to demonstrate the robustness of the intensity fluctuation approach for extracting rotational time scales in optical setups employing objectives with different NAs and consequently differing sensitivity to out-of-plane dipole orientations.

Toward this end, rotational time scales were extracted from data collected on pPDI in PS using an analogous optical setup to that used in the experiments that yielded the data in Figure 3 but using an NA = 0.95 objective lens. Median rotational time scales  $\tau_{c,LD}$  and  $\tau_{c,I}$  extracted from data collected with the NA = 0.95 objective show excellent agreement with one another in terms of temperature dependence and absolute

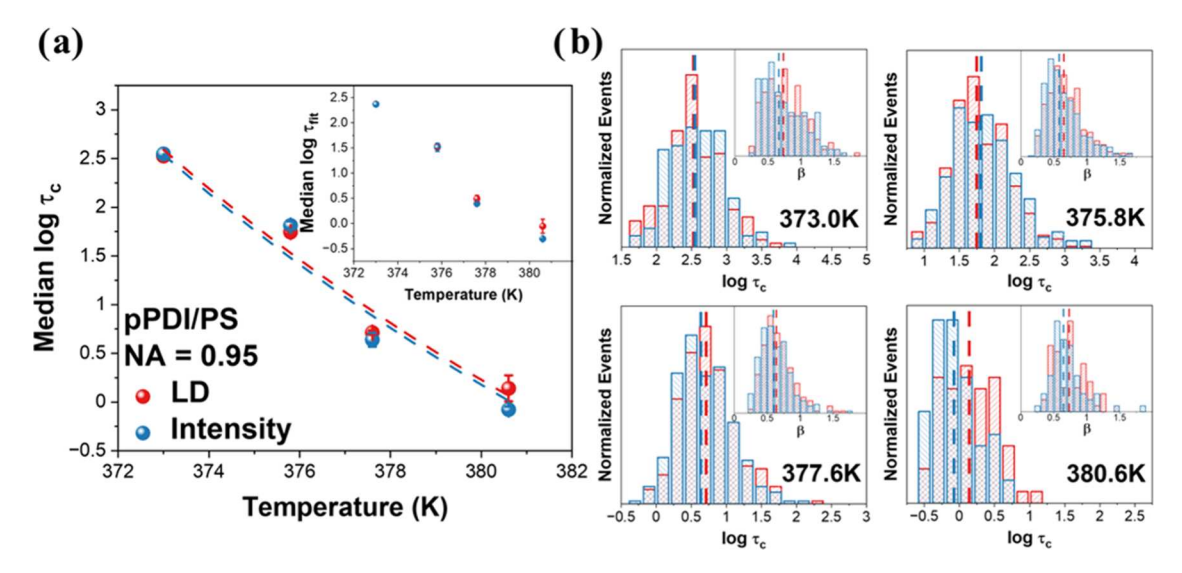


Figure 5. (a) Median  $\tau_c$  derived from LD and intensity measurements for NA = 0.95 (red and blue, respectively). Error bars are standard deviations from the movies analyzed; error bars are not present for 373.0 K data as only a single movie was collected at this temperature. The colored dashed lines are the fits of the corresponding data to this VFT equation. (b) Distributions of  $\tau_c$  and (inset)  $\beta$  values. Dashed lines indicate median values.

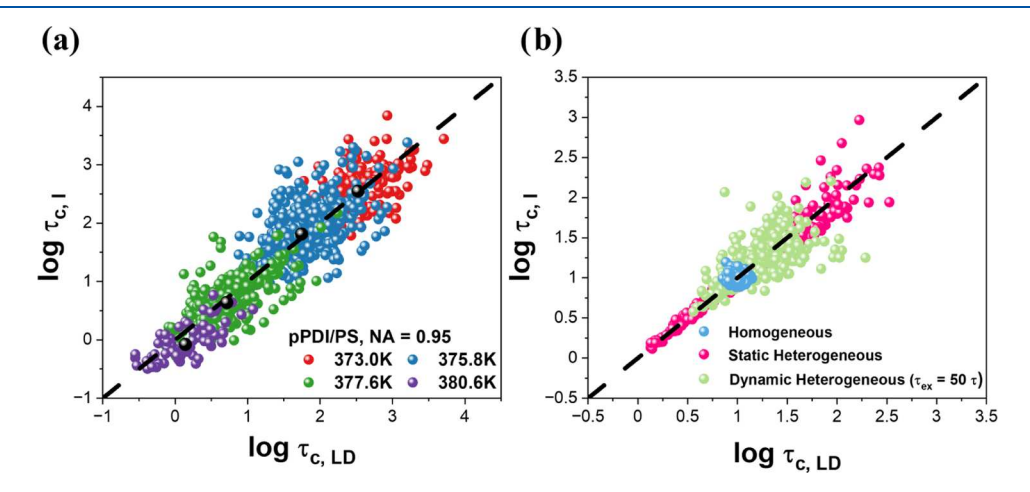


Figure 6. (a) Scatterplots of log  $\tau_{c,I}$  vs log  $\tau_{c,LD}$  for pPDI in PS for NA = 0.95. Large black dots indicate the median time scales for all features at each corresponding temperature. Pearson correlation coefficients are 0.575, 0.582, 0.669, and 0.727 for 373.0 K, 375.8 K, 377.6 K and 380.6 K respectively. (b) Scatterplots of median log  $\tau_{c,I}$  vs log  $\tau_{c,LD}$  in simulations of (pink dots) static heterogeneous and (blue dots) homogeneous dynamics compared with (lime dots) heterogeneous dynamics with exchange time ( $\tau_{ex}$ ) of 1000 frames (50  $\tau$ ). Pearson correlation coefficients of 0.973 are reported for static heterogeneous simulations while -0.053 and 0.624 are reported for homogeneous and dynamic heterogeneous simulations with  $\tau_{ex}$  = 1000 frames (50  $\tau$ ), respectively. Data for homogeneous and static heterogeneous simulations are also shown in Figure S3a, where the scatterplots are not obscured by overlaid points associated with the dynamic heterogeneous simulation.

value of the rotational correlation time (Figure 5) as well as to those obtained with the NA = 0.75 objective (Figure 3). Again, some difference at the highest temperature of 380.6 K is evident, which we attribute to experimental limitations as this data was collected at the shortest exposure time, 0.02 s, of all movies making particle tracking extremely difficult due to low signal-to-noise. However, given the overall excellent agreement across temperatures, it is apparent that LD and intensity are sampling and reporting the same rotational time scales with both NA objectives. As in the other two cases shown, distributions of  $\tau_c$  and  $\beta$  are also very similar across both techniques (Figure 5b).

Of course, the SM nature of these experiments permits access to per-probe comparisons of  $\tau_{c,LD}$  and  $\tau_{c,I}$ . This perprobe comparison returns moderate correlation, as measured by Pearson R correlation coefficients, with the NA = 0.95 optical setup returning a comparable or greater degree of

correlation at each temperature compared to the NA = 0.75 optical setup for pPDI in PS or BODIPY268 in OTP (Figures 6a and S2). It is notable that no data set exhibits Pearson R values near unity. Since the median and distributions of said time scales show good agreement, it is unlikely that a mechanistic difference between the rotations probed by each approach explains this only moderate correlation. Instead, we postulate that the extent of observed correlation is limited by the underlying heterogeneity in the system.

The majority of fluorescent probes in a heterogeneous system are expected to undergo dynamic exchange, i.e., sample several distinct time scales, consistent with median values of  $\beta$  near 0.6 for our measurements in both PS and OTP. Each of these distinct time scales is experienced for a portion of the full experimental time, and a given probe will not necessarily fully sample angles during the lifetime of a given time scale. As a thought experiment, one can imagine during a particular time

period a probe may rotate entirely in plane, leading to fluctuation in linear dichroism but not in intensity. During such a time period, angles in and out of the plane are not isotropically sampled and the assumptions that underlie the calculations of the prefactors for the different rank correlation functions do not hold i.e., a2 need not dominate autocorrelations of either LD or intensity, and Table 1 is not relevant. The individual relaxation times obtained by performing an autocorrelation over data from such a time period would clearly differ, as that constructed from intensity would not decay while that constructed from LD would. The less time the probe stays in a particular dynamic environment, the more likely such periods of nonisotropic sampling of angles occur. Stringing many such periods together will lead to full angular sampling over the full trajectory; however, with the underlying time scales putatively quite different between time periods that are temporally adjacent, this again may result in a failure to meet the assumptions underlying the calculations of  $a_2$ , homogeneous isotropic rotational diffusion through small angular changes, resulting in differences in the autocorrelations of intensity and linear dichroism from these trajectories.

To support this hypothesis, we simulated isotropic, random walks of simultaneous rotational and translational dynamics for a homogeneous case, static heterogeneous case (i.e., each feature samples a dynamic time scale from a log-normal distribution of FWHM = 1.5 and maintains this time scale indefinitely) and dynamic heterogeneous case (i.e., each feature resamples its dynamic time scale periodically over the course of the simulation). All simulations were 10,000 frames long with average  $\tau_c = 10.0$  s,  $D_t = 3.02$  nm<sup>2</sup>/s and a time between frames of 0.5 s to approximate the experimental scenario for pPDI in PS at ≈376 K. Rotational and translational dynamics were sampled independently of one another and exchanges, when relevant, occurred simultaneously. Representative simulations with static heterogeneity are shown in Videos S4 and S5. Translation was included in the simulated movies to enable simulations to be analyzed in the same manner as experimental data.

Homogeneous simulations (Figure 6b, blue dots) show a small spread of  $\tau_c$  values for both LD and intensity measurements. While there is no discernible correlation between  $au_{c,LD}$  and  $au_{c,D}$  the minor spread of these values sets a baseline expectation of the statistical limitations expected from the analyzed SM data sets. In contrast, simulations with static heterogeneity (Figure 6b, pink dots) show very high correlation in obtained  $\tau_c$  values between the two techniques, approaching near unity correlation, as is expected since each simulated molecule has sufficient time to sample all angular orientations for the single time scale experienced. Interestingly, when a simple version of dynamic heterogeneity-in the form of dynamic exchanges every 1000 frames (50  $\tau_c$ ) – is introduced, the correlation between  $au_{c,LD}$  and  $au_{c,I}$  decreases, with a result quite similar to what is seen in experiments for pPDI in PS (Figure 6b, lime dots). The correlation is partially restored if the time between exchange is extended to  $\tau_{\rm ex} = 2500$ frames (125  $\tau_c$ ) (Figure S3b, lavender dots), supporting the hypothesis that such dynamic exchange may be the underlying reason that per-molecule correlation between  $au_{c,\,\mathrm{LD}}$  and  $au_{c,I}$ shows only moderate correlation.

### CONCLUSIONS

We show that a simple approach, monitoring only singlechannel fluorescence intensity in a wide-field fluorescence

configuration, is suitable for characterizing rotational dynamics of single molecules in the complex environment of polymeric and small molecule glass formers. First, calculations show that both the linear dichroism and intensity approaches are expected to show decays dominated by the second-rank rotational correlation function for typical setups used in single molecule experiments even when limited signal or limited signal-to-noise levels affect sensitivity to probes oriented near the optical axis. However, such calculations assume small angle, isotropic rotational diffusion, which may or may not be the dominant rotational dynamics in certain probe/host systems. Despite this, we find that rotational time scales extracted from intensity fluctuations report near identical absolute time scales, temperature dependence, and degrees of heterogeneity to those extracted from the commonly used linear dichroism approach across both the probe/host systems and optical configurations examined. Finally, we show the correlation between rotational relaxation times obtained from linear dichroism and intensity on a per-probe basis is consistent with the presence of dynamic heterogeneity, which limits the time frame over which angular orientations are sampled for each time scale experienced. The intensity-based approach presented here is compelling due to its simplicity and its ability to retain photons otherwise lost in more complex experimental schemes, thus preserving localization precision and facilitating measurements that benefit from simultaneous rotational and translational characterization.

## ASSOCIATED CONTENT

# Supporting Information

The Supporting Information is available free of charge at https://pubs.acs.org/doi/10.1021/acs.jpcb.4c02097.

Correlation function prefactors for an oil immersion objective, figures showing native one channel results on pPDI in PS, scatterplots of  $\tau_{\rm c,I}$  vs  $\tau_{\rm c,LD}$  for pPDI/PS and B268/OTP, and scatterplots of  $\tau_{\rm c,I}$  vs  $\tau_{\rm c,LD}$  for simulated systems with dynamic heterogeneity and  $\tau_{\rm ex}=2500$  frames (PDF)

Representative movie of pPDI in PS collected at 375.8 K with NA = 0.75 and an exposure time of 2 s (MP4)

Representative movie of B268 in OTP collected at 244.5 K with NA = 0.75 and an exposure time of 3 s (MP4)

Representative movie of pPDI in PS collected at 375.8 K with NA = 0.95 and an exposure time of 2 s (MP4)

Representative simulated two channel movie of static heterogeneous dynamics. Simulations were output as two, orthogonally polarized channels and book matched to create two channel images (MP4)

Representative simulated single channel movie of static heterogeneous dynamics. Simulations were output as two, orthogonally polarized channels and summed to create single channel images (MP4)

#### AUTHOR INFORMATION

#### **Corresponding Author**

Laura J. Kaufman — Department of Chemistry, Columbia University, New York, New York 10027, United States; orcid.org/0000-0002-3754-0831; Email: kaufman@chem.columbia.edu

#### Authors

 Alec R. Meacham – Department of Chemistry, Columbia University, New York, New York 10027, United States
 Jaladhar Mahato – Department of Chemistry, Columbia University, New York, New York 10027, United States
 Han Yang – Department of Chemistry, Columbia University, New York, New York 10027, United States

Complete contact information is available at: https://pubs.acs.org/10.1021/acs.jpcb.4c02097

#### **Notes**

The authors declare no competing financial interest.

## ACKNOWLEDGMENTS

This work was supported by the National Science Foundation under awards CHE-2246765 and CHE-1954803. We thank Prof. Keewook Paeng and Dr. Nicole L. Mandel for helpful discussions.

#### REFERENCES

- (1) Ediger, M. D. Spatially Heterogeneous Dynamics in Supercooled Liquids. *Annu. Rev. Phys. Chem.* **2000**, *51* (1), 99–128.
- (2) Ediger, M. D.; Angell, C. A.; Nagel, S. R. Supercooled Liquids and Glasses. J. Phys. Chem. A 1996, 100 (31), 13200-13212.
- (3) Richert, R. Heterogeneous Dynamics in Liquids: Fluctuations in Space and Time. *J. Phys.: Condens. Matter* **2002**, *14* (23), R703–R738.
- (4) Cicerone, M. T.; Ediger, M. D. Relaxation of Spatially Heterogeneous Dynamic Domains in Supercooled Ortho-terphenyl. *J. Chem. Phys.* **1995**, *103* (13), 5684–5692.
- (5) Kaufman, L. J. Heterogeneity in Single-Molecule Observables in the Study of Supercooled Liquids. *Annu. Rev. Phys. Chem.* **2013**, 64 (1), 177–200.
- (6) Deschenes, L. A.; Vanden Bout, D. A. Heterogeneous Dynamics and Domains in Supercooled *o* -Terphenyl: A Single Molecule Study. *J. Phys. Chem. B* **2002**, *106* (44), 11438–11445.
- (7) Adhikari, A. N.; Capurso, N. A.; Bingemann, D. Heterogeneous Dynamics and Dynamic Heterogeneities at the Glass Transition Probed with Single Molecule Spectroscopy. *J. Chem. Phys.* **2007**, *127*, No. 114508.
- (8) Paeng, K.; Kaufman, L. J. Single Molecule Experiments Reveal the Dynamic Heterogeneity and Exchange Time Scales of Polystyrene near the Glass Transition. *Macromolecules* **2016**, *49* (7), 2876–2885.
- (9) Paeng, K.; Park, H.; Hoang, D. T.; Kaufman, L. J. Ideal Probe Single-Molecule Experiments Reveal the Intrinsic Dynamic Heterogeneity of a Supercooled Liquid. *Proc. Natl. Acad. Sci. U.S.A.* **2015**, 112 (16), 4952–4957.
- (10) Mackowiak, S. A.; Herman, T. K.; Kaufman, L. J. Spatial and Temporal Heterogeneity in Supercooled Glycerol: Evidence from Wide Field Single Molecule Imaging. *J. Chem. Phys.* **2009**, *131* (24), No. 244513
- (11) Pramanik, R.; Ito, T.; Higgins, D. A. Single Molecule Wobbling in Cylindrical Mesopores. *J. Phys. Chem. C* **2013**, *117*, 3668–3673.
- (12) Pramanik, R.; Ito, T.; Higgins, D. A. Molecular Length Dependence of Single Molecule Wobbling within Surfactant- and Solvent-Filled Silica Mesopores. *J. Phys. Chem. C* **2013**, *117*, 15438–15446.
- (13) Nordén, B. Applications of Linear Dichroism Spectroscopy. *Appl. Spectrosc. Rev.* **1978**, *14* (2), 157–248.
- (14) Paeng, K.; Kaufman, L. J. Which Probes Can Report Intrinsic Dynamic Heterogeneity of a Glass Forming Liquid? *J. Chem. Phys.* **2018**, *149*, No. 164501.
- (15) Blackburn, F. R.; Wang, C.-Y.; Ediger, M. D. Translational and Rotational Motion of Probes in Supercooled 1,3,5-Tris(Naphthyl)-Benzene. *J. Phys. Chem. A* **1996**, *100*, 18249–18257.
- (16) Chang, I.; Fujara, F.; Geil, B.; Heuberger, G.; Mangel, T.; Sillescu, H. Translational and Rotational Molecular Motion in

- Supercooled Liquids Studied by NMR and Forced Rayleigh Scattering. J. Non-Cryst. Solids 1994, 172–174, 248–255.
- (17) Cicerone, M. T.; Ediger, M. D. Enhanced Translation of Probe Molecules in Supercooled O-Terphenyl: Signature of Spatially Heterogeneous Dynamics? *J. Chem. Phys.* **1996**, *104* (18), 7210–7218
- (18) Cicerone, M. T.; Blackburn, F. R.; Ediger, M. D. Anomalous Diffusion of Probe Molecules in Polystyrene: Evidence for Spatially Heterogeneous Segmental Dynamics. *Macromolecules* **1995**, 28 (24), 8224–8232.
- (19) Mandel, N. L.; Lee, S.; Kim, K.; Paeng, K.; Kaufman, L. J. Single Molecule Demonstration of Debye-Stokes-Einstein Breakdown in Polystyrene near the Glass Transition Temperature. *Nat. Commun.* **2022**, *13*, No. 3580.
- (20) Wang, M.; Marr, J. M.; Davanco, M.; Gilman, J. W.; Liddle, J. A. Nanoscale Deformation in Polymers Revealed by Single-Molecule Super-Resolution Localization—Orientation Microscopy. *Mater. Horiz.* **2019**, *6*, 817—825.
- (21) Zhang, O.; Guo, Z.; He, Y.; Wu, T.; Vahey, M. D.; Lew, M. D. Six-Dimensional Single-Molecule Imaging with Isotropic Resolution Using a Multi-View Reflector Microscope. *Nat. Photonics* **2023**, *17*, 179–186.
- (22) Thompson, R. E.; Larson, D. R.; Webb, W. W. Precise Nanometer Localization Analysis for Individual Fluorescent Probes. *Biophys. J.* **2002**, *82*, 2775–2783.
- (23) Ober, R. J.; Ram, S.; Ward, E. S. Localization Accuracy in Single-Molecule Microscopy. *Biophys. J.* **2004**, *86* (2), 1185–1200.
- (24) Fourkas, J. T. Rapid Determination of the Three-Dimensional Orientation of Single Molecules. *Opt. Lett.* **2001**, 26 (4), 211–213.
- (25) Wei, C.-Y. J.; Kim, Y. H.; Darst, R. K.; Rossky, P. J.; Vanden Bout, D. A. Origins of Nonexponential Decay in Single Molecule Measurements of Rotational Dynamics. *Phys. Rev. Lett.* **2005**, *95*, No. 173001.
- (26) Berne, B. J.; Pecora, R. Dynamic Light Scattering: With Applications to Chemistry, Biology, and Physics; John Wiley & Sons: New York. 1976.
- (27) Hinze, G.; Diezemann, G.; Basche, Th. Rotational Correlation Functions of Single Molecules. *Phys. Rev. Lett.* **2004**, 93, No. 203001.
- (28) Backlund, M. P.; Lew, M. D.; Backer, A. S.; Sahl, S. J.; Moerner, W. E. The Role of Molecule Dipole Orientation in Single-Molecule Fluorescence Microscopy and Implications for Super-Resolution Imaging. *ChemPhysChem* **2014**, *15*, 587–599.
- (29) Lu, C.-Y.; Vanden Bout. Analysis of Orientational Dynamics of Single Fluorophore Trajectories from Three-Angle Polarization Experiments. *J. Chem. Phys.* **2008**, *128*, No. 244501.
- (30) Toprak, E.; Enderlein, J.; Syed, S.; McKinney, S. A.; Petschek, R. G.; Ha, T.; Goldman, Y. E.; Selvin, P. R. Defocused Orientation and Position Imaging (DOPI) of Myosin V. *Proc. Natl. Acad. Sci. U.S.A.* **2006**, *103* (17), 6495–6499.
- (31) Uji-i, H.; Melnikov, S. M.; Deres, A.; Bergamini, G.; De Schryver, F.; Herrmann, A.; Mullen, K.; Enderlein, J.; Hofkens, J. Visualizing Spatial and Temporal Heterogeneity of Single Molecule Rotational Diffusion in a Glassy Polymer by Defocused Wide-Field Imaging. *Polymer* **2006**, *47*, 2511–2518.
- (32) Reznik, C.; Berg, R.; Foster, E.; Advincula, R.; Landes, C. F. Transient Three-Dimensional Orientation of Molecular Ions in an Ordered Polyelectrolyte Membrane. *J. Phys. Chem. Lett.* **2011**, 2 (6), 592–598.
- (33) Chung, I.; Shimizu, K. T.; Bawendi, M. G. Room Temperature Measurements of the 3D Orientation of Single CdSe Quantum Dots Using Polarization Microscopy. *Proc. Natl. Acad. Sci. U.S.A.* **2003**, *100* (2), 405–408.
- (34) Ha, T.; Laurence, T. A.; Chemla, D. S.; Weiss, S. Polarization Spectroscopy of Single Fluorescent Molecules. *J. Phys. Chem. B* **1999**, 103 (33), 6839–6850.
- (35) Herman, T. K.; Mackowiak, S. A.; Kaufman, L. J. High Power Light Emitting Diode Based Setup for Photobleaching Fluorescent Impurities. *Rev. Sci. Instrum.* **2009**, *80*, No. 016107.

- (36) Paeng, K.; Swallen, S. F.; Ediger, M. D. Direct Measurement of Molecular Motion in Freestanding Polystyrene Thin Films. *J. Am. Chem. Soc.* **2011**, *133* (22), 8444–8447.
- (37) Mackowiak, S. A.; Kaufman, L. J. When the Heterogeneous Appears Homogeneous: Discrepant Measures of Heterogeneity in Single-Molecule Observables. *J. Phys. Chem. Lett.* **2011**, *2*, 438–442.
- (38) Schneider, C. A.; Rasband, W. S.; Eliceiri, K. W. NIH Image to Image]: 25 Years of Image Analysis. *Nat. Methods* **2012**, *9*, 671–675.
- (39) Hoang, D. T.; Paeng, K.; Park, H.; Leone, L. M.; Kaufman, L. J. Extraction of Rotational Correlation Times from Noisy Single Molecule Fluorescence Trajectories. *Anal. Chem.* **2014**, *86* (18), 9322–9329.
- (40) Sbalzarini, I. F.; Koumoutsakos, Pl. Feature Point Tracking and Trajectory Analysis for Video Imaging in Cell Biology. *J. Struct. Biol.* **2005**, *151* (2), 182–195.
- (41) Virtanen, P.; Gommers, R.; Oliphant, T. E.; Haberland, M.; Reddy, T.; Cournapeau, D.; Burovski, E.; Peterson, P.; Weckesser, W.; Bright, J.; et al. SciPy 1.0: Fundamental Algorithms for Scientific Computing in Python. *Nat. Methods* **2020**, *17* (3), 261–272.
- (42) Seabold, S.; Perktold, J. In *Statsmodels: Econometric and Statistical Modeling with Python*; Proceedings of the 9th Python in Science Conference, 2010; pp 92–96.
- (43) Stokely, K.; Manz, A. S.; Kaufman, L. J. Revealing and Resolving Degeneracies in Stretching Exponents in Temporally Heterogeneous Environments. J. Chem. Phys. 2015, 142, No. 114504.
- (44) Bell, T. D. M.; Stefan, A.; Masuo, S.; Vosch, T.; Lor, M.; Cotlet, M.; Hofkens, J.; Bernhardt, S.; Mullen, K.; Auweraer, M. V. D.; et al. Electron Transfer at the Single-Molecule Level in a Triphenylamine-Perylene Imide Molecule. *ChemPhysChem* **2005**, *6*, 942–948.
- (45) Hoogenboom, J. P.; van Dijk, E. M. H. P.; Hernando, J.; van Hulst, N. F.; Garcia-Parajo, M. F. Power-Law-Distributed Dark States Are the Main Pathway for Photobleaching of Single Organic Molecules. *Phys. Rev. Lett.* **2005**, *95*, No. 097401.
- (46) Lu, H. P.; Xie, X. S. Single-Molecule Spectral Fluctuations at Room Temperature. *Nature* **1997**, *385*, 143–146.
- (47) Vogel, H. The Temperature-Dependent Viscosity Law for Liquids. *Phys. Z.* **1921**, *22*, 645–646.
- (48) Fulcher, G. S. Analysis of Recent Measurements of the Viscosity of Glasses. J. Am. Ceram. Soc. 1925, 8 (16), 339-355.
- (49) Tammann, G.; Hesse, W. The Dependence of Viscosity on Temperature in Supercooled Liquids. *Z. Anorg. Allg. Chem.* **1926**, 156 (1), 245–257.
- (50) Roland, C. M.; Casalini, R. Temperature Dependence of Local Segmental Motion in Polystyrene and Its Variation with Molecule Weight. *J. Chem. Phys.* **2003**, *119*, 1838–1842.
- (51) Lu, C.-Y.; Vanden Bout, D. A. Effect of Finite Trajectory Length on the Correlation Function Analysis of Single Molecule Data. *J. Chem. Phys.* **2006**, *125*, No. 124701.
- (52) Richert, R. On the Dielectric Susceptibility Spectra of Supercooled O-Terphenyl. J. Chem. Phys. 2005, 123, No. 154502.